Chemical Engineering & Processing: Process Intensification 148 (2020) 107802

Contents lists available at ScienceDirect

Chemical Engineering & Processing: Process Intensification

journal homepage: www.elsevier.com/locate/cep

Enhanced transport in Gas-Liquid-Solid catalytic reaction by structured wetting properties: Nitrite hydrogenation

Pengyu Xu[a], Shilpa Agarwal[b], Jimmy Faria Albanese[a], Leon Lefferts[a,*]

[a] Catalytic Processes and Materials Group, Faculty of Science and Technology, MESA+ Institute for Nanotechnology, University of Twente, PO Box 217, 7500 AE Enschede, the Netherlands

[b] Infineum UK Ltd, Milton Hill Business & Technology Centre, PO Box 1, Abingdon, Oxfordshire, OX13 6BB, UK

ARTICLE INFO

Keywords:
Nitrite hydrogenation
Partially hydrophobic
Pd/γ-Al_2O_3aqueous phase
Mass transfer

ABSTRACT

This work presents a new approach to improve mass transfer in and around catalyst particles in three-phase operation with micro-structured catalysts, containing hydrophilic and hydrophobic domains. Partially hydrophilic catalysts were prepared via physical mixing of hydrophobic perfluorinated octyltrichloro silane (FOTS)/γ-Al_2O_3 domains and hydrophilic Pd/γ-Al_2O_3 domains, resulting in manipulation of water wetting, both at the external surface and the pores inside the support particles. The modified catalysts were characterized with elemental analysis, XRF, N_2 physisorption and light microscopy after selective dyeing hydrophobic and hydrophilic domains. The catalysts are tested for hydrogenation of nitrite in water, which is an extremely fast reaction whereas the product distribution (N_2 versus NH_4^+) is also easily influenced by internal concentration gradients. Noticeably, the partially hydrophilic catalyst is more active and produces more ammonium compared to hydrophilic catalyst. This work demonstrates that this way of structuring the catalyst enables influencing the internal concentration gradients for aqueous systems. For the case of nitrite hydrogenation, we show that structured catalysts achieve the same rate per gram Pd at lower hydrogen pressure compared to classical hydrophilic catalysts. This results in formation of less ammonia, which is of practical importance for cleaning of drinking water.

1. Introduction

Nitrate contamination of groundwater, caused by landfills, livestock, over-fertilization and industry, is an emergent problem in the supply of safe drinking water [1–3]. Nitrate can be converted in the human body to more toxic nitrite, decreasing the oxygen transport capacity of blood especially in infants. Moreover, nitrite can react with amines and amides, resulting in carcinogenic N-nitroso compounds [4–8]. Therefore, the European Environment Agency has established its legal limits for nitrate and nitrite at 50 and 0.1 mg/L, respectively [9].

Nitrate and nitrite contaminants can be removed from water by several techniques, such as biological denitrification, ion exchange and catalytic hydrogenation. Biological denitrification is not applicable for drinking water, due to the low concentration of nutrients to sustain the growth of bacteria [5]. Ion exchange results in formation of a concentrated brine that cannot be easily discharged [5]. A promising strategy to convert these nitrates and nitrites is the catalytic reduction towards nitrogen with molecular hydrogen [1,10–24]. The reactions involved in nitrite hydrogenation are presented in Eqs. (1) and (2). For practical applications, the selectivity to N_2 must be almost complete in order to prevent formation of ammonia as its permitted concentration (0.5 mg/L) in drinking water is even lower than that of nitrates (50 mg/L).

$$2NO_2^- + 3H_2 + 2H^+ \xrightarrow{Catalyst} N_2 + 4H_2O \quad (1)$$

$$NO_2^- + 3H_2 + 2H^+ \xrightarrow{Catalyst} NH_4^+ + 2H_2O \quad (2)$$

Transport of hydrogen to the catalyst in a slurry reactor is schematically shown in Fig. 1, top of the figure. Hydrogen first dissolves in water at the gas-liquid interface and diffuses through the stagnant liquid film at the gas-liquid interface. The bulk of the water is well mixed and dissolved hydrogen diffuses through the stagnant liquid film at the outside of the catalyst support particles, followed by diffusion into the pores of the catalyst support, before reaching the active site. The catalyst is completely wetted with water and the pores are completely filled with water. In contrast, transport of nitrite and protons proceeds via diffusion from the bulk of the liquid, via the stagnant liquid film at the external catalyst surface, to the active sites inside the pores. The

* Corresponding author.
E-mail address: l.lefferts@utwente.nl (L. Lefferts).

https://doi.org/10.1016/j.cep.2020.107802
Received 29 October 2019; Received in revised form 17 December 2019; Accepted 6 January 2020
Available online 11 January 2020

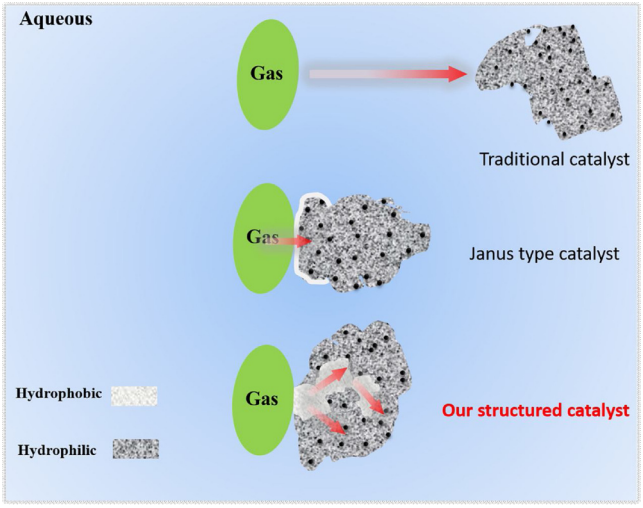

Fig. 1. Schematic representation of the concept of the interaction of catalyst containing hydrophobic domains with gas bubbles in water (bottom), compared to a traditional hydrophilic catalyst (top) and a Janus particle with hydrophobicity exclusively at the external surface (middle).

transport of hydrogen in water is generally more sluggish though, due to its low solubility. The consequence is that active sites in the catalyst support particles may be exposed to different nitrite, proton (pH) and hydrogen concentrations, resulting in lower reaction rates and changes in selectivity of the reaction [25]. It is generally accepted that the ammonium selectivity depends on the ratio of NO_2^-/H_2 at the active site, influencing the concentration of adsorbed species on the Pd surface [12]; formation of ammonia is minimal by minimizing the H_2 concentration. Unfortunately, too low H_2 concentration would also induce very low rates, because of kinetics and because of internal H_2 mass transfer limitation. Internal concentration gradients are undesired, causing variation in both selectivity to ammonia as well as activity on Pd particles, depending on the location in the catalyst support. The main challenge is to achieve a relatively low hydrogen concentration at all active sites, so that all active sites can operate at conditions close to the optimal NO_2^-/H_2 ratio with the optimal balance between activity and selectivity.

For this reason, usually slurry phase reactors are used [15,25,26] as internal mass transfer limitations can be partly suppressed by using small catalyst support particles. In contrast, trickle bed reactors may be more practical [27] but suffer more from internal diffusion limitations because of the larger support particle size. Recently, we demonstrated that a membrane contactor reactor [14,28] is favorable for this purpose, enabling operation at low hydrogen pressure without affecting the rate of reaction because of transport limitations.

An alternative approach to alleviate this problem is presented in Fig. 1, bottom of the figure, in which the catalyst wettability is tailored to enhance transport of gaseous reactants towards the active sites, without sacrificing the accessibility of the reactants in aqueous phase. In this strategy, a fraction of the catalyst surface (external and internal) is selectively hydrophobized to enable direct contact with the gas bubbles, providing a rapid transport pathway for hydrogen. The remaining fraction of the catalyst is kept hydrophilic to facilitate transport of nitrite to the active sites. A key element in this approach is to restrict the spatial distribution of the metal clusters to the hydrophilic domains of the catalyst to ensure the accessibility of the active sites to the aqueous reactants. In this way, the gas-liquid interface is positioned inside the catalyst particles resulting in much shorter diffusion lengths of hydrogen dissolved in water.

Partially hydrophobic support materials have been explored previously [29–33]. “Janus” type of catalyst particles (The middle catalyst in Fig. 1) have been developed to increase the external mass transfer in liquid-liquid phase systems [33–35], e.g. enhancing transport of 4-tert-butoxystyrene in water phase during hydrogenation. Note that in this case the catalyst particles are dense and only external surface is modified. Quintanilla et al. [31] reported that introducing hydrophobicity to a Pd/SiO_2 catalyst for hydrogenation of aromatic ketones, decreased the adsorption strength of alcohol on the surface of the support, thus suppressing consecutive hydrogenation to saturated alcohol. Thus, enhancing internal and external mass transfer via modification of both the internal and external surface of porous catalysts has not been reported before to the best of our knowledge, except for our previous work described below.

In our previous work, we reported on the influence of partial hydrophobization of $Pd/\gamma\text{-}Al_2O_3$ on the catalytic activity and selectivity of nitrite hydrogenation in a slurry reactor [14]. In that case, we compared the performance of fully hydrophilic $Pd/\gamma\text{-}Al_2O_3$ with two distinct types of partially hydrophobic catalysts. One type was prepared by physically mixing and pelletizing small particles of hydrophilic $Pd/\gamma\text{-}Al_2O_3$ and hydrophobic $\alpha\text{-}Al_2O_3$, resulting in catalysts containing well-defined hydrophilic and hydrophobic domains. The other type consisted of $Pd/\gamma\text{-}Al_2O_3$ functionalized with varying amounts of perfluorinated-octyltrichlorosilane. The catalytic experiments showed that the activity slightly increased when the catalyst was partially hydrophobized, regardless of the strategy employed to introduce hydrophobicity. Notably, the selectivity towards ammonia increased from 15 % in the case of hydrophilic $Pd/\gamma\text{-}Al_2O_3$ to 20 and 30 % for the catalyst made via physical mixing of hydrophilic and hydrophobic domains and for the $Pd/\gamma\text{-}Al_2O_3$ catalyst modified partially with FOTS, respectively. The system was not buffered, causing unfavorable high selectivity to ammonium due to pH gradients inside catalyst particles. The further increase in ammonia selectivity was rationalized in terms of local changes in the concentration of hydrogen relative to nitrite at the active sites inside the catalyst particles, due to enhanced transport of the hydrogen in the partially hydrophobic catalysts. However, further increase of the hydrophobicity of the catalysts lead to significant mass transport limitations of the nitrite ions dissolved in the aqueous phase, which negatively affected the activity. Although the change in selectivity is unfavorable in view of application, the results demonstrated that internal transport can be manipulated.

In this work, we report on the effect of hydrogen and nitrite concentration on the performance of catalysts containing hydrophobic and hydrophilic domains. The concept is explained in Fig. 1, showing that gas bubbles will not only interact with the hydrophobic parts of the external surface, but will also fill the pores in the hydrophobic domains with gas. As a result, a gas-liquid interface exists inside the catalyst particles, resulting in extremely short diffusion pathways in wetted pores. We will test the hypothesis that a partially hydrophilic catalyst can operate at lower hydrogen pressure with the same activity and at the same time lower selectivity to ammonia, compared to a classical hydrophilic catalyst. In addition, the influence of the support particle size as well as the ratio between hydrophilic and hydrophobic domains will be discussed. All experiments are performed in the presence of CO_2 as a buffer, in order to achieve favorable low selectivity to ammonium.

2. Experimental section

2.1. Materials

Commercial $\gamma\text{-}Al_2O_3$ powder (surface area 198 m^2/g) was purchased from BASF. Palladium precursor tetraamminepalladium (II) nitrate solution (10 wt% in H_2O, 99.99 %), Trichloro(1H,1H,2H,2H-perfluorooctyl)silane ($(CF_3(CF_2)_5CH_2CH_2SiCl_3$, FOTS, 97 %), n-hexane, sodium nitrite (99.99 %, used as source for nitrite ions (NO_2^-)), ammonium (50 % v/v water) were obtained from Sigma-Aldrich. Methylene blue hydrate ($C_{16}H_{20}ClN_3OS$, pure) was purchased from ACROS Organics. All the aqueous solutions were prepared using ultra purified water obtained with a water purification system (Millipore,

Synergy).

2.2. Catalyst preparation

2.2.1. Parent catalyst hydrophilic Pd/γ-Al_2O_3 synthesis

The Pd/γ-Al_2O_3 (1 wt%) catalyst was prepared via wet impregnation. Typically 10 g of the sieved alumina support (particle size less than 38 μm, mean particle size is 22 μm ± 0.1 as measured with dynamic light scattering method) was calcined at 600 °C for 4 h to remove any organic contaminants. Then the support was suspended in 100 mL millQ water. The pH of the solution was adjusted around 9 by adding 2 mL ammonia solution, in order to ensure electrostatic interaction of $Pd(NH_3)_4^{2+}$ with the negatively charged alumina surface. Subsequently, 3 g of the palladium precursor solution (3.3 wt%) was slowly added to the suspension. The final suspension was stirred at room temperature for at least 1 h and then transferred to a rotary evaporator to remove the liquid at 70 °C under vacuum. Finally, the catalyst was calcined in air (flow rate 30 mL/min) at 400 °C for 3 h (heating rate 5 °C/min), and subsequently reduced in 50 vol% H_2 diluted in N_2 (total flow rate 60 mL/min) at the same temperature for 3 h.

2.2.2. Parent catalyst hydrophobic FOTS/γ-Al_2O_3 synthesis

γ-Al_2O_3 is hydrophobized by introducing FOTS according to a procedure described in detail elsewhere[30]. In short, 1.5 g of γ-Al_2O_3 (after pretreatment as described above, particles smaller than 38 μm) was added to 40 mL solution of FOTS dissolved in hexane (25 mM) and the mixture was stirred for 10, 30, 60 or 120 min. The solvent was removed by filtration followed by drying in a vacuum oven at 100 °C for 1 h, improving the bonding of FOTS to the support. The sample was rinsed with hexane to remove any physisorbed FOTS.

2.2.3. Partially hydrophilic catalyst synthesis

Partially hydrophilic catalysts were prepared by physical mixing of hydrophilic Pd/γ-Al_2O_3 and hydrophobic FOTS/γ-Al_2O_3, followed by pressing, breaking and sieving. A single batch of Pd/γ-Al_2O_3 was used as the parent hydrophilic catalyst. In addition, physical mixing avoids contact between FOTS and the Pd particles. Therefore, the dispersion of the Pd is constant in all experiments. The percentage of hydrophilic domains is expressed as weight percentage, which was varied between 20 % and 80 %. As an example, the 50 % hydrophilic catalyst was prepared by mixing 0.5 g hydrophobized FOTS/γ-Al_2O_3 with 0.5 g Pd/γ-Al_2O_3. The mixture was pressurized at 4000 bar for 2 min in a cold isostatic press. The pressurized pellet was broken and sieved to obtain samples with particle sizes in the windows 0–38, 45–100, 200–250, 250–300 and 300–425 μm.

2.3. Catalyst characterization

2.3.1. Parent catalyst hydrophilic Pd/γ-Al_2O_3

The BET surface area of the hydrophilic catalyst, degassed at 300 °C for 1 day, was determined with N_2-adsorption at 77 K (Micromeritics Tristar). The Pd loading on the alumina support was determined with X-ray fluorescence spectroscopy (XRF, Philips PW 1480). Pd particle size was determined using TEM (Tecnai F30), measuring at least 300 Pd particles at ten different spots in the catalyst. X-ray diffraction (XRD, Bruker D2 Phaser diffractometer), with Cu Kα radiation (λ = 0.1544 nm) was used to identify the phases present in the samples. The metal surface area that is accessible was determined with CO chemisorption at room temperature (Chemisorb 2750, Micromeritics). Typically, the sample was reduced at room temperature in hydrogen for 1 h and flushed with He at the same temperature for 0.5 h. Then, CO was introduced as pulses and the response was recorded using a TCD detector. Pd particle sizes are estimated assuming hemispherical metal particles and assuming that the stoichiometric ratio of adsorbed CO and Pd surface atoms is one. The mean catalyst support particle size was measured with dynamic light scattering (DLS) method using a Malvern Mastersizer 2000 with Hydro 2000S module.

2.3.2. Parent catalyst hydrophobic FOTS/γ-Al_2O_3

The thermal stability of FOTS on alumina was determined using thermo-gravimetrical analysis (TGA/SDTA851e, Mettler Toledo). Briefly, the sample was heated in 30 mL/min Ar flow to the target temperature varying between 100 °C and 300 °C, with a heating rate of 5 °C/min. The target temperature was maintained for 1 h, followed by cooling down to room temperature. The BET surface area of the hydrophobic catalyst (after degassing at 135 °C for 1 day) was determined with N_2-adsorption 77 K (Micromeritics Tristar). The amount of FOTS on the surface was calculated based on elemental analysis (CHNS-O Analyzer, Interscience, Thermo Scientific) according Eq. (3):

$$SC\left(\frac{mol\ FOTS}{m^2}\right) = \%C * \frac{1}{100} * \frac{g\ C}{g\ total} * \frac{1\ mol\ C}{12\ g\ C} * \frac{1\ mol\ FOTS}{8\ mol\ C} * \frac{1\ g\ total}{BET\ m^2} \quad (3)$$

where SC is the surface coverage of FOTS, %C is the carbon weight concentration as obtained from the elemental analysis and BET is the surface area of the material according to N_2 physisorption; the factor 8 originates from the number of carbon atoms in FOTS.

2.3.3. Partially hydrophilic catalyst

To determine qualitatively the hydrophobicity of the materials, contact angle measurements were performed on a pellet of the sample. Even though surface roughness of the pellet will influence the contact angles, the method still indicates trends in hydrophobicity. The water contact angle was measured using an OCA 15 Dataphysics. Scanning Electron Microscopy (JEOL, JSM-6490) was used to study the catalyst surface morphology. Coverage with FOTS and Pd loading were determined via elemental analysis and XRF respectively, as described above. The catalyst support particle size of both fresh and spent catalyst was measured by dynamic light scattering (DLS) Malvern Mastersizer 2000 with Hydro 2000S module.

2.4. Catalytic tests

Activity and selectivity of the catalysts were measured in a 1 L batch reactor operated at 20 °C, atmospheric pressure and a pH value of 5.5, maintained by buffering continuously with CO_2 (0.1 bar). The glass reactor (DURAN® BAFFLED, WIDE MOUTH BOTTLE GLS 80®) has a diameter of 10.1 cm and height 22.2 cm (Figure S1). The reactor has four connections on the reactor lid for gas-in, gas-out, sampling and a stirring shaft equipped with 4 stirring blades. Internal and external mass transfer limitation are examined on both experiments as well as calculations as described in details in the supporting information section mass transfer checking.

Typically, 0.05 g catalyst was suspended in 0.3 L millQ water and stirred at 700 rpm under 0.8 bar hydrogen (0.1 bar CO_2, 0.1 bar He) to remove oxygen and to reduce the catalyst for at least 1 h. Reaction was started on introduction of 3 mL $NaNO_2$ solution (100 mmol/L). The hydrogen pressure was varied between 0.1 and 0.8 bar, and the nitrite concentration was varied between 0.3 and 1 mmol/L. Table 1 presents detailed reaction conditions.

Samples were taken at different reaction times using a 2.5 mL syringe (BD Plastipak) and filtered through a syringe filter (PTFE, 0.2 μm, Whatman) in order to remove the catalyst. Nitrite and ammonium concentrations were measured with ion-chromatography (DIONEX, ICS 3000) equipped with an UltiMate autosampler.

NO_2^- conversion and integral NH_4^+ selectivity were calculated according to Eqs. (4) and (5), respectively. Since it is well known that ammonia and nitrogen are the only products formed during hydrogenation of nitrite [21,36–39], nitrogen was calculated based on the mass balance. Since the formation rate of the N_2 is not practical to measure under our conditions, we calculated conversion and selectivity

Table 1
Operating conditions of the nitrite hydrogenation in slurry reactor.

Reaction temperature, °C	20
Reaction volume, L	0.3
pH of the solution	5.5
Stirring speed, rpm	700
Tested partially hydrophilic catalyst particle size, μm	100 - 250
Amount of catalyst, g	0.03
Initial nitrite concentration, mmol/L	1
Total gas flow rate, mL/min	100
Total operating pressure, bar	1
Carbon dioxide partial pressure, bar	0.1
Hydrogen partial pressure, bar	0.1 - 0.8
Helium partial pressure (balance), bar	0.1 - 0.8

based on the nitrite and ammonium concentration in the liquid.

$$NO_2^- \text{ conversion} = \frac{[NO_2^-]_{t0} - [NO_2^-]_{t1}}{[NO_2^-]_{t0}} * 100 \quad (4)$$

$$\text{Integral } NH_4^+ \text{ selectivity} = \frac{[NH_4^+]_{t1}}{[NO_2^-]_{t0} - [NO_2^-]_{t1}} * 100 \quad (5)$$

Where $[NO_2^-]_{t0}$ is the initial nitrite concentration, $[NO_2^-]_{t1}$ is the concentration of nitrite at t1, $[NH_4^+]_{t1}$ is the concentration of ammonium at t1.

Differential ammonium selectivity was calculated according to Eq. (6).

$$\text{Differential } NH_4^+ \text{ selectivity} = \frac{[\text{formation rate } NH_4^+]_{t1}}{[\text{conversion rate } NO_2^-]_{t1}} * 100 \quad (6)$$

Where formation rate of NH_4^+ rate is calculated based on the polynomial fitting equation at t1, differential NO_2^- rate is also calculated according to the polynomial fitting equation at t1. Figure S2 shows a typical fitting example. It is noticeable that the polynomial fitting is used in all the experiments.

The apparent turn-over-frequency (TOF) was calculated based on differential NO_2^- rate at t1, according Eq. (7).

$$TOF = \frac{[\text{conversion rate } NO_2^-]_{t1} \; mol*s^{-1}}{\text{moles of available surface Pd mol}} \quad (7)$$

where the number of available Pd surface-atoms was obtained with CO-chemisorption.

3. Results and discussion

3.1. Catalyst preparation and characterization

3.1.1. Parent hydrophilic catalyst: Pd/γ-Al_2O_3

Table 2 shows the characterization results of the hydrophilic parent catalyst. The XRF results confirm that the Pd loading is close to the 1 wt % target. Also, deposition of Pd does not influence the BET surface area as well as the pore volume, indicating that the support structure remains unchanged.

Furthermore, the crystal structure of pure alumina support and Pd-loaded support was measured with XRD. Figure S3 shows that the diffractogram remains unchanged during catalyst preparation and no palladium diffraction peaks were detected, suggesting that Pd is highly dispersed. Indeed, CO chemisorption (Table 1) confirms high Pd dispersion (56 %) in Pd/γ-Al_2O_3, which is equivalent to an averaged metal particle size of 2 nm. This is also in reasonable agreement with the HRTEM images, shown in Fig. 2b as a typical example. The particle size distribution based on multiple micrographs is presented in Fig. 2c, resulting in an averaged Pd particle size of 2.2 nm.

3.1.2. Parent hydrophobic catalyst: FOTS/γ-Al_2O_3

The hydrophobic alumina particles were prepared via silane functionalization using FOTS. Fig. 3a shows that 30 min of reaction of γ-Al_2O_3 with FOTS is already sufficient to saturate the carbon content at about 6.7 wt%. Surface density of FOTS is 3.5 μmol/m^2 as calculated based on Eq. (3). This is in good agreement with literature [40], indicating that γ-Al_2O_3 has been fully hydrophobized via reaction of FOTS with the hydroxyl groups on the surface of the alumina (see Figure S3).

The thermal stability of the FOTS was tested with TGA in Ar atmosphere up to 800 °C. Fig. 3b shows the weight loss profile of FOTS/γ-Al_2O_3, showing significant weight loss centered at 300 °C in contrast with results on bare γ-Al_2O_3. In order to determine the temperature window in which the samples are not affected, TGA experiments were performed using different final temperatures. Fig. 3c shows that the weight loss is below 3 % for temperatures below 150 °C, indicating that the FOTS is stable on the alumina surface at that temperature. Based on these results, the samples were degassed at 135 °C before N_2-physisorption measurements. The surface area presented in Table 2, obtained with the Brunauer–Emmett–Teller (BET) method, for the FOTS/γ-Al_2O_3 was 112 m^2/g, which is significantly smaller than the surface area of Pd/γ-Al_2O_3. The reduction in the surface area upon FOTS functionalization was also accompanied by a 50 % decrease in pore volume compared to Pd/γ-Al_2O_3 (Table 2), in agreement with the pore-size distribution presented in Figure S5, using the Barrett, Joyner, and Halenda method (BJH). Introduction of FOTS decreases the accessibility of the pores, which are typically smaller than 20 nm, probably due to due to partial pore filling as well as pore blockage [25].

3.1.3. Partially hydrophilic catalyst

The partially hydrophilic catalysts were prepared by mixing hydrophilic Pd/γ-Al_2O_3 and hydrophobic FOTS/γ-Al_2O_3 in different mass ratios (1:0, 4:1, 3:2, 1:1, 2:3 and 1:4; Pd/γ-Al_2O_3:FOTS/γ-Al_2O_3) followed by pelletizing at 4000 bar. The high pressure is intended to create strong mechanical binding between the hydrophilic and hydrophobic materials, minimizing catalyst attrition during reaction. Catalyst particle sizes distribution determined both before and after catalyst testing are presented in Figure S7, confirming that the level of attrition is not significantly influencing the catalytic results. The morphology of the partially hydrophilic catalysts was examined with SEM (Fig. 4), showing no differences in morphology between Pd/γ-Al_2O_3 and FOTS/γ-Al_2O_3 particles in Fig. 4a and b. In previous work in our group [25] two distinct surface topologies were observed by SEM after palletizing a mixture of Pd supported on γ-Al_2O_3 and FOTS-containing α-Al_2O_3, thanks to the different surface morphologies of the parent materials (e.g. γ- and α-Al_2O_3). Unfortunately, this is not possible for the samples in this study. Notably, inspection at higher magnification of the 20 % partially hydrophilic catalyst (Fig. 4 c and d) confirms the absence of

Table 2
Characterization data of both parent catalysts, hydrophilic (Pd/γ-Al_2O_3), hydrophobic (FOTS/γ-Al_2O_3) and support material γ-Al_2O_3.

		Elemental analysis	N_2 physisorption		XRF	CO-chemisorption
Sample	Particle size (μm)	Carbon (wt%)	Specific surface area (m^2/g)	Pore volume (cm^3/g)	Pd loading (wt%)	Pd dispersion (%)
γ-Al_2O_3	0 - 38	n/a	198	0.67	n/a	n/a
Pd/γ-Al_2O_3	0 - 38	0.4	193	0.63	0.9	56
FOTS/γ-Al_2O_3	0 - 38	7.1	112	0.29	n/a	n/a

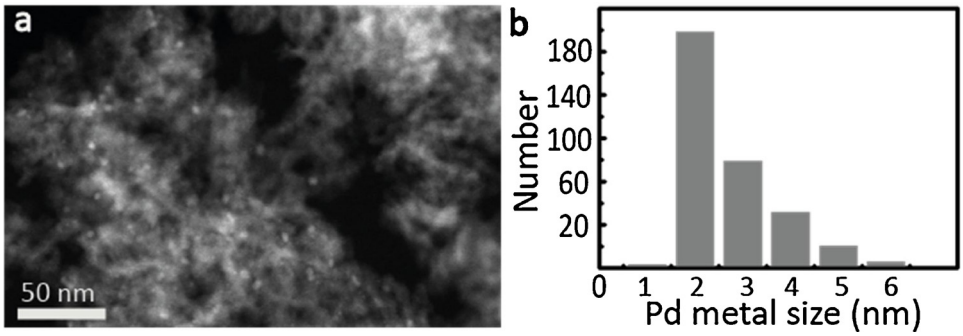

Fig. 2. a) TEM image of the Pd/γ-Al_2O_3 catalyst particles, the bright spots are Pd metal particles, b) Pd metal size distribution based on 300 particle sizes.

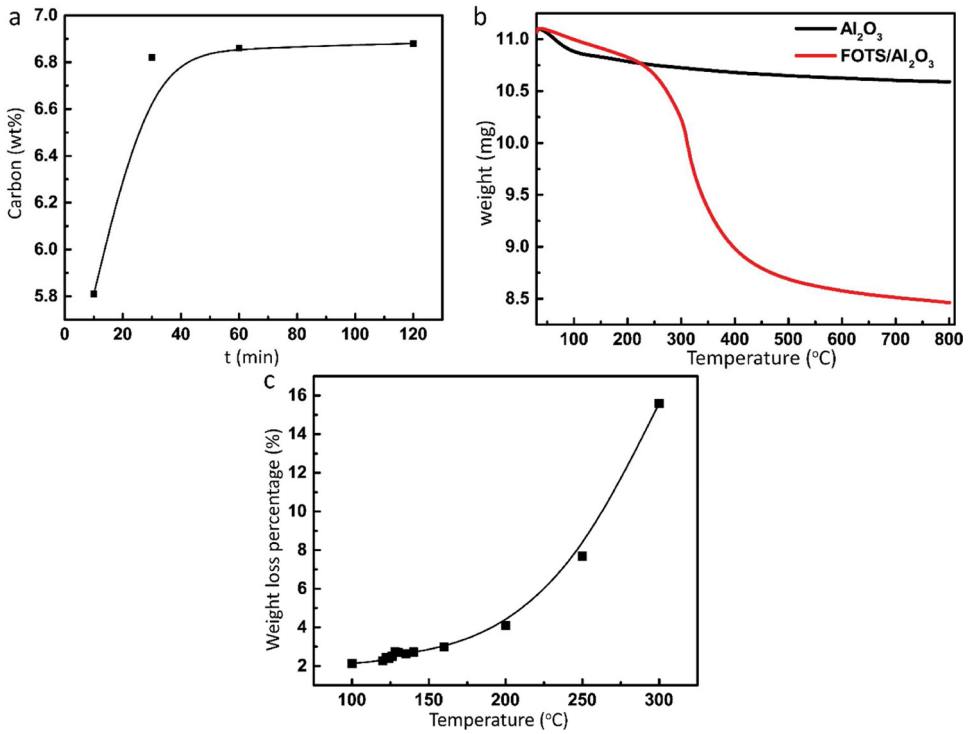

Fig. 3. a) Influence of synthesis time on carbon concentration of FOTS/γ-Al_2O_3 measured by elemental analysis, b) TGA profile of FOTS/γ-Al_2O_3 in the temperature range of 25–800 °C (10 °C/min, 30 mL/min Ar), c) weight loss of FOTS/γ-Al_2O_3 as result of a TGA experiment with different final temperatures (30 mL/min Ar, 10 °C/min, 1 h at final temperature).

any macro-porosity between parent particles with maximum size of 38 μm. Similar results were obtained for the 80 % and 50 % hydrophilic catalyst (see Figure S6). The distribution of hydrophilic domains in the catalyst is visualized with Methylene-blue (Figure S6c), wetting exclusively the hydrophilic domains. This confirms the presence of well-distributed hydrophilic domains at the surface of the catalyst particles. The size of the domains is similar to the size of the hydrophilic parent catalyst particles (Table 3).

Notably, increasing the content of hydrophobic FOTS/γ-Al_2O_3 leads to decreasing specific surface areas, pore volume and Pd loading and increasing carbon concentration. All these properties change linearly with the fraction of hydrophilic catalyst, as expected assuming the preparation procedure is well controlled and that the 100–250 μm fraction has the same composition as the initial mixture of hydrophilic and hydrophobic catalysts (Fig. 5). Furthermore, the high-pressure treatment employed to create the partially hydrophilic catalysts did not change the surface area significantly (Table S1), indicating that the support structure was retained.

Fig. 6 shows the same trend qualitatively for the contact angle of water droplets measured on the mechanically fabricated pellets of the partially hydrophilic catalysts. The contact angle increases significantly from 40° to 143° with increasing content of the hydrophobic parent catalyst, confirming that the hydrophobicity of the catalyst can be tuned by simply varying the ratio of Pd/γ-Al_2O_3 and FOTS/γ-Al_2O_3.

Table 4 shows the carbon concentrations measured on different particle sizes after crushing and sieving. Clearly, the composition of the catalyst does not vary with the particle size, when keeping the ratio of hydrophilic and hydrophobic parent catalyst constant. Thus, all fractions contained the same ratio of hydrophobic and hydrophilic domains, indicating that the particles of the two parent catalysts were homogeneously distributed in the pellet of the partially hydrophilic catalysts, before crushing. Also, the experimental values of the carbon concentration agree very well with the value expected based on the ratio of hydrophilic and hydrophobic parent catalyst.

Similar results were obtained based on the Pd content as measured with XRF, as shown in Table 5 for the 80 % hydrophilic catalyst. Although the metal loading was slightly lower than the theoretical value, the variation with particle size is not significant. This confirms that hydrophilic and hydrophobic domains are homogeneously distributed over the fractions with different particles sizes.

3.2. Catalytic performance

Fig. 7 (black line) shows that the apparent initial TOF of the fully hydrophilic catalyst decreases with increasing catalyst particle size. Mass transfer limitation is dominating the rate of reaction when the

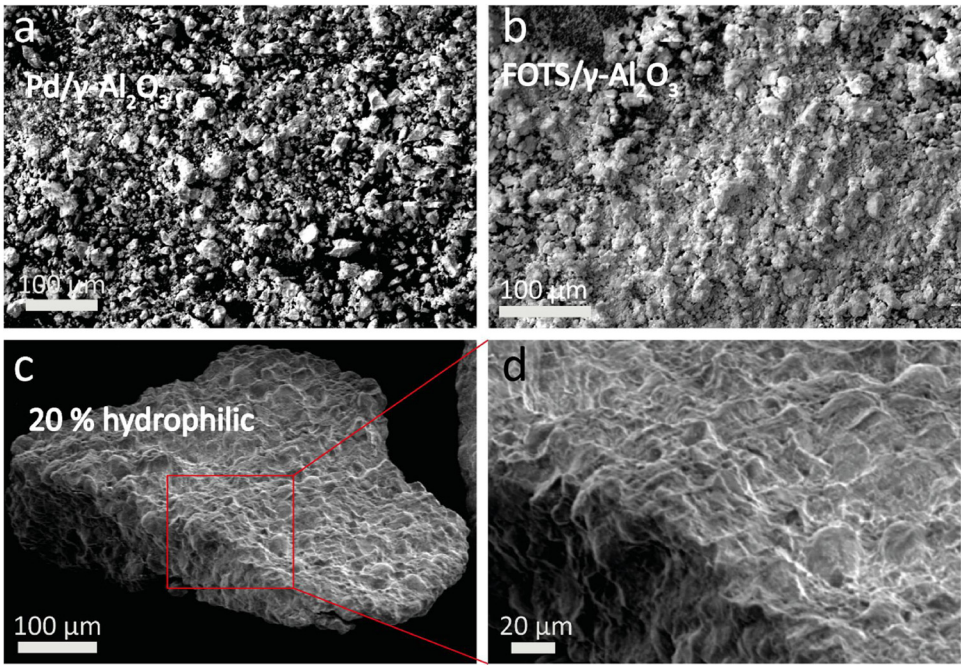

Fig. 4. SEM image of a) Pd/γ-Al_2O_3 (0–38 µm), b) FOTS/γ-Al_2O_3 (0–38 µm), SEM image of a partially hydrophilic catalyst particle (300–425 µm) c) mixing 20 % Pd/γ-Al_2O_3 with 80 % FOTS/γ-Al_2O_3, d) the zoom-in of the particles shown in c.

Table 3
Characterization of partially hydrophilic catalyst with different ratio and particle size between 100 and 250 µm: BET surface, pore volume, carbon concentration and Pd loading.

sample	BET surface area (m^2/g)	Pore volume (cm^3/g)	Carbon (wt %)	Pd loading (wt%)
100 % hydrophilic	184	0.41	0.4	1.1
80 % hydrophilic	167	0.35	1.4	0.7
50 % hydrophilic	152	0.29	3.4	0.5
20 % hydrophilic	131	0.23	5.5	0.2

particle size is larger than 100 µm. Calculation of the Weisz-Prater criteria (Table S2) confirms that catalyst particle larger than 100 µm results in severe mass transfer limitation for both hydrogen and nitrite. In contrast, the small catalyst particles are much more active and the Weisz-Prater criterion confirms that the rate is determined by kinetics only. The observed activity, 12 mol*s^{-1}*mol^{-1} Pd_s, is in good agreement with our previous work reporting on intrinsic kinetics [41]. The activity also agrees in order of magnitude with other studies, although it should be noted that precise comparison is not possible because of differences in experimental conditions [42,43].

Fig. 7 (red line) shows that the 80 % hydrophilic catalyst with particle size between 100–250 µm is significantly more active than the hydrophilic catalyst with the same particle size. No difference in activity is observed between the two types of catalysts with particles smaller than 100 µm, which is easily understood as internal diffusion limitation is not significant and therefore hydrophilic-hydrophobic structuring cannot enhance the reaction rate. This is in agreement with the results of Franch et al. [25], reporting minor or no effect of similar hydrophilic-hydrophobic structuring on the reaction rate when using catalyst particle size between 40 and 100 µm.

Surprisingly, also the larger particles between 300 and 425 µm show similar activity for fully hydrophilic and partially hydrophobic catalyst. As shown in Figure S6c, the hydrophilic and hydrophobic domains are randomly distributed throughout the catalyst particles. Therefore, we propose that a significant fraction of the hydrophilic Pd/γ-Al_2O_3 domains are completely surrounded by FOTS/γ-Al_2O_3 domains, which cannot contribute to any activity as the active sites are not accessible for nitrite ions. The larger the catalyst particles, the more Pd/γ-Al_2O_3 domains are likely isolated. This adverse effect probably compensates the enhancement of mass transfer, increasing the activity. Therefore, catalysts with the particle size between 100 and 250 µm were selected for further catalytic testing.

Fig. 8 shows the effect of the hydrophilic/hydrophobic ratio on the initial catalytic activity (expressed as apparent TOF, mole nitrite per

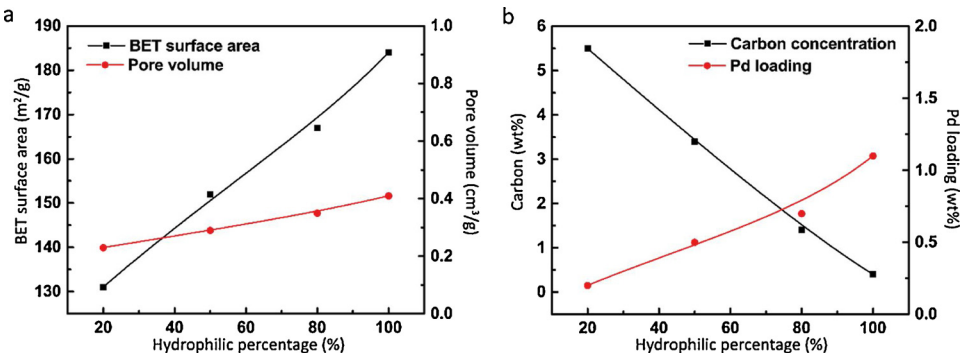

Fig. 5. a) BET surface area, pore volume, b) carbon concentration and Pd loading as a function of the percentage of hydrophilicity.

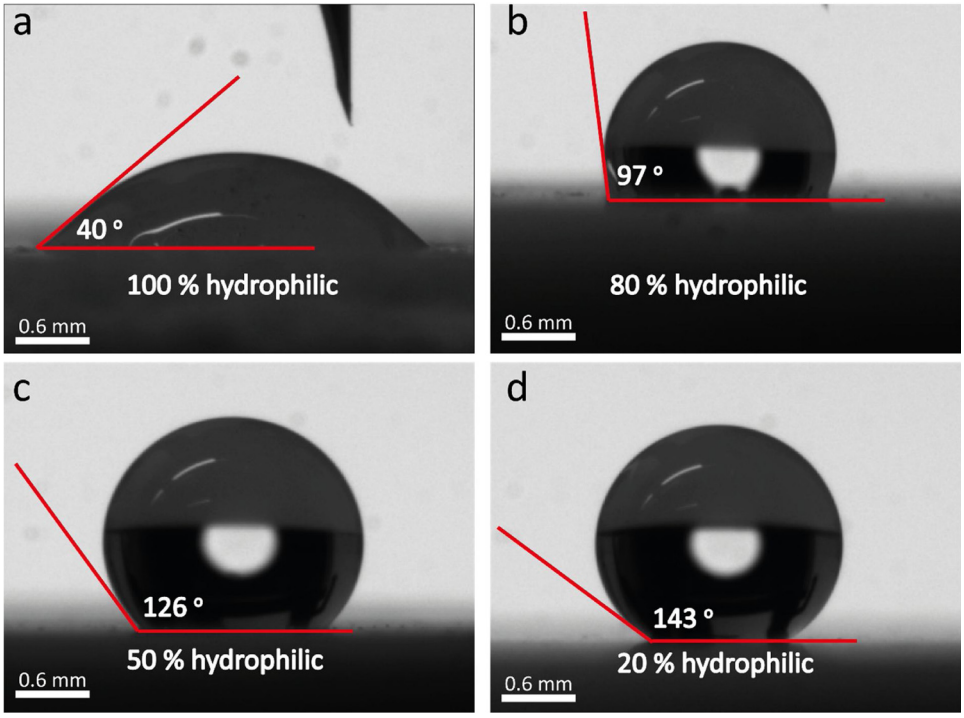

Fig. 6. The contact angle pictures, a) fully hydrophilic, b) 80 % hydrophilic, c) 50 % hydrophilic, d) 20 % hydrophilic pelletized samples.

Table 4
Variation in carbon concentration in partially hydrophilic catalyst with particle size and ratio of hydrophilic and hydrophobic parent catalyst.

Sample	Particle size (μm)			
	100 -250	250 - 300	300 - 425	Theoretical[a]
80 % hydrophilic	1.4	1.4	1.4	1.4
60 % hydrophilic	2.6	2.7	2.7	2.9
50 % hydrophilic	3.4	3.5	3.7	3.6
40 % hydrophilic	4.3	4.3	4.2	4.3
20 % hydrophilic	5.5	5.8	5.8	5.7

[a] Theoretical value calculated based on the composition of mixture.

Table 5
The distribution of Pd loading in different particles size in 80 % hydrophilic catalyst.

Sample	Particle size (μm)			
	100 - 250	250 - 300	300 - 425	Theoretical[a]
80 % hydrophilic	0.7 ± 0.1	0.6 ± 0.1	0.7 ± 0.1	0.88

[a] Theoretical value were calculated based on the mixture of the parents ratio (80 %).

mole surface Pd), resulting in a volcano-like plot. The error margin is determined by multiple repetition of the experiment with 80 % hydrophilic catalyst. The 80 % hydrophilic catalyst is significantly more active than the fully hydrophilic catalyst. The activity decreases on further decreasing the hydrophilicity to 50 % and 20 %; note that a pure hydrophobic catalyst has no activity because it does not contain any Pd. Nevertheless, all partially hydrophilic catalyst are more active per mole surface-Pd and therefore utilize the active sites better then fully hydrophilic catalysts, which is attributed to enhancement of hydrogen transport to the active sites. The smaller effect on the 20 % and 50 % hydrophilic catalyst is probably caused by flotation during catalyst testing as observed visually. Mal-distribution of the catalyst in the reactor apparently compensates partly the favorable effect of hydrophilic-

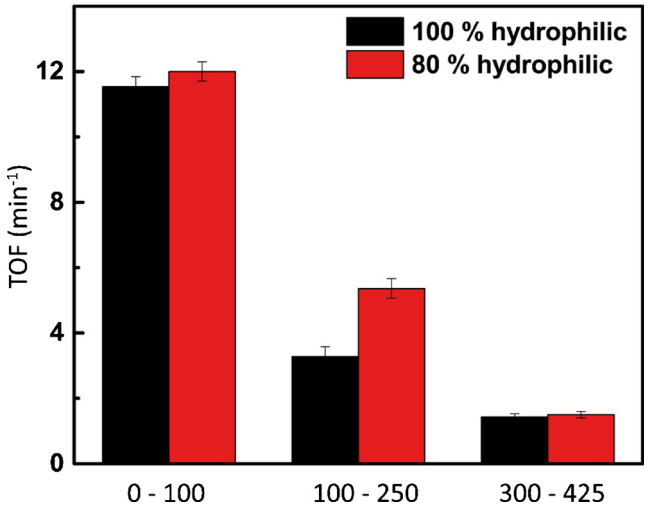

Fig. 7. Initial apparent TOF measured on different catalyst particle size for 100 % hydrophilic catalyst and 80 % hydrophilic catalyst (30 mg catalyst, 0.3 mM NO_2^-, 0.8 bar H_2, 0.1 bar CO_2, 20 °C).

hydrophobic structuring.

Fig. 9a, S9a and S10a show that the 80 % hydrophilic catalyst is noticeable more active than the 100 % hydrophilic catalyst independent of hydrogen pressure, in agreement with Fig. 8. Fig. 9a, S9a and S10a also show that activity increases with the hydrogen partial pressure for both catalysts, in general agreement with literature [11,21,36,39,44]. Both observations are valid for varying nitrite concentrations, as a result of varying nitrite conversion of 0 %, 20 % and 40 % in respectively Figs. 9a, S9a and S10a.

Figure S8 shows experimental results on the formation of ammonium as function of nitrite conversion. The ammonium concentration increases with conversion for all the samples, due to the fact that ammonium cumulates in the batch experiment. Note that a small amount of ammonium is produced at the very beginning of the experiment. The absolute amount is constant, i.e. 0.88 μmol in all experiments. This

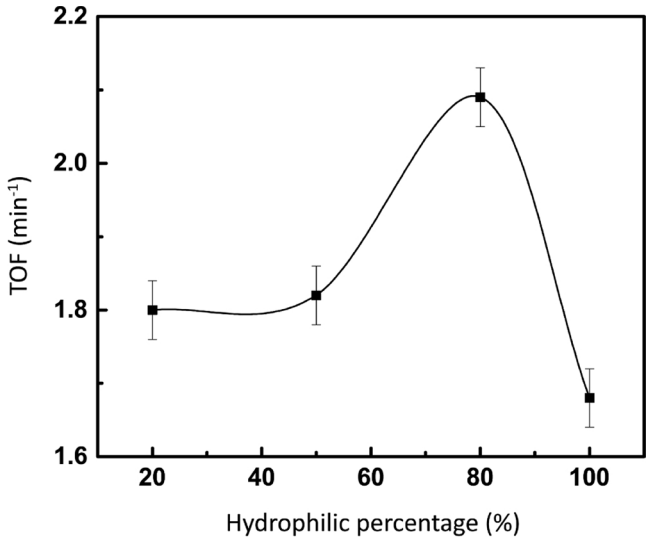

Fig. 8. Influence of the percentage of hydrophilicity on the apparent TOF calculated based on initial rate of nitrite conversion for particles in the window 100 – 250 µm (30 mg catalyst, 0.3 mM NO_2^-, 0.8 bar H_2, 0.1 bar CO_2, 20 °C).

effect is attributed to the presence of excess hydrogen on the Pd catalyst when starting the experiment by injecting the nitrite solution, as the catalyst is reduced in-situ before. Formation of the observed amount of ammonium requires 15.8 µmol atomic H, which is equivalent to 15 % of the ML capacity. Nevertheless, selectivity to ammonium is less than 5 % in all experiments, in agreement with others studies from our group [45,46] and by others [42,43], provided that the pH is buffered with CO_2. In contrast, selectivity to ammonium can be as high as 50 % when pH changes during reaction are not buffered [11–13,25,36,44],

In all cases, catalysts for nitrite hydrogenation are tested in slurry batch experiments, resulting in integral ammonium selectivity, i.e. based on the cumulative amount of ammonia formed according Eq. 5. Continuous operation is clearly favored for practical operation. The performance of a trickle-bed reactor in plug-flow regime is equivalent to a batch reactor, be it that variation in time in the batch reactor is equivalent to variation in residence time along the axis in a fixed bed reactor, under the condition that the hydrogen pressure is constant. In that case, the cumulative selectivity to ammonia is to be considered, after subtraction of the amount of ammonia formed immediately at the start as discussed above. Please note that the integral ammonium selectivity reported in Figure S9c, S9f, S10c and S10f for different nitrite concentration and conversion, have been corrected accordingly.

In case of a continuous stirred tank reactor (CSTR), the selectivity is determined by the conditions in the outlet of the reactor and the selectivity is determined by the ratio of the rates of formation of N_2 and ammonium at those conditions. We term this as differential ammonium selectivity (Eq. 6). Fig. 9b, S9b and S10b present the differential ammonium selectivity as function of the hydrogen pressure at different nitrite conversion level, which is also a measure for the nitrite concentration, calculated according Eq. 6. Clearly, integral and differential selectivity to ammonia increase with hydrogen partial pressure (Fig. 9b, S9b, S9c, S10b, and S10c). Figure S8 shows clearly that the selectivity to ammonia also increases with decreasing nitrite concentration, which can also be seen by comparing Figs. 9b, S9b and S10b. These effects can be explained based on NO_2^-/H_2 ratio; higher ratios result in less ammonia formation [25].

Partially hydrophilic catalysts exhibit higher ammonium selectivity, both integral (Figure S9c and S10c) as well as differential (Fig. 9b, S9b and S10b) in all cases, due to enhanced hydrogen mass transfer, thus increasing the hydrogen/nitrite ratio. The same trend was observed by Franch et al. [25], despite the smaller catalyst particles used (45–100 µm) and absence of any significant effect on activity.

Thus, partly hydrophobizing the catalyst enhances activity, at the expense of undesired increasing selectivity to ammonia. In other words, partly hydrophobic catalyst can achieve the same space-time-yield and equally efficient use of Pd as hydrophilic catalyst at lower hydrogen

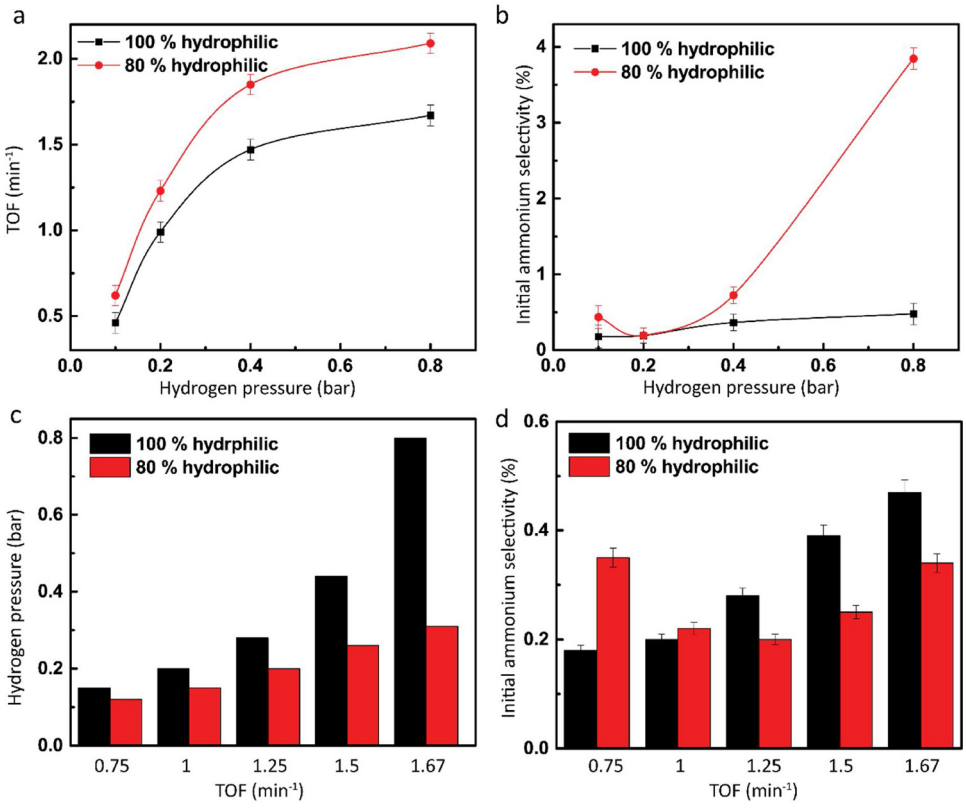

Fig. 9. a) Influence of the hydrogen pressure on the initial apparent TOF for 100 % hydrophilic (black line) and 80 % hydrophilic (red line) catalyst, b) initial ammonium selectivity (differential ammonium selectivity) as function of hydrogen pressure for 100 % hydrophilic (black line) and 80 % hydrophilic (red line) catalyst (30 mg catalyst, 1 mM NO_2^-, 0.8 bar H_2, 0.1 bar CO_2, 20 °C), c) the required hydrogen pressures to achieve identical TOF levels on 100 % hydrophilic and 80 % hydrophilic catalyst, d) the resulting ammonium selectivity (For interpretation of the references to colour in this figure legend, the reader is referred to the web version of this article).

pressure. We will now discuss whether we can use this phenomenon to suppress ammonia formation in both plug flow reactors and CSTR reactors.

In the case of CSTR operation, considering differential ammonium selectivity, lower hydrogen pressure is sufficient for partially hydrophilic catalyst to achieve the same TOF as hydrophilic catalyst at higher hydrogen pressure (Fig. 9c). This effect is the largest when operating at high TOF. Fig. 9d presents the selectivity to ammonia for both catalysts when operating at the same TOF, at hydrogen pressures as discussed above. Remarkably, partially hydrophilic catalyst has lower selectivity to ammonium than hydrophilic catalyst when operating at high TOF, i.e. using the Pd catalyst most efficiently. The effect reverts when operating at unfavorable low TOF. Importantly, these effects are observed independent of nitrite conversion, i.e. nitrite concentration (Figure S9d, S9e, S10d and S10e).

A very similar result is obtained when considering operation in a plug flow trickle-bed reactor. Figure S9f and S10f present the integral ammonium selectivity for both catalysts operating at the same TOF, by selecting hydrogen pressures as discussed above. The trends for the integral and differential ammonium selectivity are similar. Thus, also in this case the partially hydrophilic catalyst produces less ammonium compared to hydrophilic catalyst, when operating at high TOF.

Qualitatively, this result can be understood by considering that internal concentration gradients are more dominant in hydrophilic supports. Operation at high apparent TOF then requires high hydrogen pressure, which causes high selectivity to ammonium, especially at the outer shell of the catalyst particles. In contrast, a partly hydrophilic catalyst develops less internal concentration gradients, lower hydrogen concentration is required to achieve the same activity and especially the outer shell of the catalyst operates at much lower hydrogen concentration. The result is a decreased selectivity to ammonium. This work demonstrates that it is possible to manipulate the performance of supported catalysts in three-phase operation in water, via structuring the catalysts in terms or wettability, both at the internal and external surface of the support. Additional work is required to use the same principle in combination with other solvents.

4. Conclusion

Catalysts containing hydrophilic and hydrophobic domains have been prepared with well controlled ratio of the amount of hydrophobic domains and hydrophilic domains, independent of the particle size. Noticeably, the partially hydrophilic catalyst is more active and produces more ammonium compared to hydrophilic catalyst. This demonstrates that internal concentration gradients are indeed influenced. For the case of nitrite hydrogenation, we conclude that structured catalysts achieve the same rate per gram Pd at lower hydrogen pressure compared to classical hydrophilic catalysts. This results in formation of less ammonia, which is of practical importance for cleaning of drinking water.

CRediT authorship contribution statement

Pengyu Xu: Methodology, Validation, Investigation, Resources, Data curation, Writing - original draft, Visualization, Funding acquisition. **Shilpa Agarwal:** Formal analysis, Writing - review & editing, Supervision. **Jimmy Faria Albanese:** Formal analysis, Writing - review & editing, Visualization, Supervision. **Leon Lefferts:** Conceptualization, Writing - review & editing, Visualization, Supervision, Project administration, Funding acquisition.

Declaration of Competing Interest

The authors declare that they have no known competing financial interests or personal relationships that could have appeared to influence the work reported in this paper.

Acknowledgments

The authors gratefully acknowledge financial support from China Scholarship Council. The microscopy works have been conducted in the "Laboratorio de Microscopias Avanzadas" at "Instituto de Nanociencia de Aragon - Universidad de Zaragoza". Authors acknowledge the LMA-INA for offering access to their instruments and expertise. We are grateful to K. Altena–Schildkamp and T.M.L Velthuizen for chemical analysis. We acknowledge B. Geerdink for technical support.

Appendix A. Supplementary data

Supplementary material related to this article can be found, in the online version, at doi:https://doi.org/10.1016/j.cep.2020.107802.

References

[1] A.J. Lecloux, Chemical, biological and physical constrains in catalytic reduction processes for purification of drinking water, Catal. Today 53 (1999) 23–34, https://doi.org/10.1016/S0920-5861(99)00100-5.
[2] V. Matějů, S. Čižinská, J. Krejčí, T. Janoch, Biological water denitrification-a review, Enzyme Microb. Technol. 14 (1992) 170–183, https://doi.org/10.1016/0141-0229(92)90062-S.
[3] G. Gulis, M. Czompolyova, J.R. Cerhan, An ecologic study of nitrate in municipal drinking water and cancer incidence in Trnava District, Slovakia, Environ. Res. 88 (2002) 182–187, https://doi.org/10.1006/enrs.2002.4331.
[4] S. Hôrold, T. Tacke, K.D. Vorlop, Catalytical removal of nitrate and nitrite from drinking water: 1. Screening for hydrogenation catalysts and influence of reaction conditions on activity and selectivity, Environ. Technol. (United Kingdom) 14 (1993) 931–939, https://doi.org/10.1080/09593339309385367.
[5] A. Kapoor, T. Viraraghavan, Nitrate removal from drinking water—review, J. Environ. Eng. (New York) 123 (1997) 371–380, https://doi.org/10.1061/(ASCE)0733-9372(1997)123:4(371).
[6] J. Martínez, A. Ortiz, I. Ortiz, State-of-the-art and perspectives of the catalytic and electrocatalytic reduction of aqueous nitrates, Appl. Catal. B Environ. 207 (2017) 42–59, https://doi.org/10.1016/j.apcatb.2017.02.016.
[7] H.O.N. Tugaoen, S. Garcia-Segura, K. Hristovski, P. Westerhoff, Challenges in photocatalytic reduction of nitrate as a water treatment technology, Sci. Total Environ. 599–600 (2017) 1524–1551, https://doi.org/10.1016/j.scitotenv.2017.04.238.
[8] S. Tyagi, D. Rawtani, N. Khatri, M. Tharmavaram, Strategies for Nitrate removal from aqueous environment using nanotechnology: a review, J. Water Process Eng. 21 (2018) 84–95, https://doi.org/10.1016/j.jwpe.2017.12.005.
[9] E.E.A. (EEA), Nitrate Concentration in Groundwater, (2002).
[10] A. Bothner-By, L. Friedman, The reaction of nitrous acid with hydroxylamine, J. Chem. Phys. 20 (1952) 459–462, https://doi.org/10.1063/1.1700442.
[11] A. Pintar, G. Berčič, J. Levec, Catalytic liquid-phase nitrite reduction: kinetics and catalyst deactivation, AIChE J. 44 (1998) 2280–2292, https://doi.org/10.1002/aic.690441017.
[12] J.K. Chinthaginjala, L. Lefferts, Support effect on selectivity of nitrite reduction in water, Appl. Catal. B Environ. 101 (2010) 144–149, https://doi.org/10.1016/j.apcatb.2010.09.023.
[13] J.K. Chinthaginjala, J.H. Bitter, L. Lefferts, Thin layer of carbon-nano-fibers (CNFs) as catalyst support for fast mass transfer in hydrogenation of nitrite, Appl. Catal. A Gen. 383 (2010) 24–32, https://doi.org/10.1016/j.apcata.2010.05.013.
[14] H.C. Aran, J.K. Chinthaginjala, R. Groote, T. Roelofs, L. Lefferts, M. Wessling, R.G.H.H. Lammertink, Porous ceramic mesoreactors: a new approach for gas–liquid contacting in multiphase microreaction technology, Chem. Eng. J. 169 (2011) 239–246, https://doi.org/10.1016/j.cej.2010.11.005.
[15] Y. Zhao, J.A. Baeza, N. Koteswara Rao, L. Calvo, M.A. Gilarranz, Y.D. Li, L. Lefferts, Unsupported PVA- and PVP-stabilized Pd nanoparticles as catalyst for nitrite hydrogenation in aqueous phase, J. Catal. 318 (2014) 162–169, https://doi.org/10.1016/j.jcat.2014.07.011.
[16] R. Brunet Espinosa, L. Lefferts, Ni in CNFs: highly active for nitrite hydrogenation, ACS Catal. 6 (2016) 5432–5440, https://doi.org/10.1021/acscatal.6b01375.
[17] J.J.F. Scholten, metal surface area and metal dispersion in catalysts, Stud. Surf. Sci. Catal. (1979), pp. 685–714, https://doi.org/10.1016/S0167-2991(09)60244-5.
[18] A. Obuchi, S. Naito, T. Onishi, K. Tamaru, Mechanism of catalytic reduction of NO by H2 or CO on a Pd foil; role of chemisorbed nitrogen on Pd, Surf. Sci. 122 (1982) 235–255, https://doi.org/10.1016/0039-6028(82)90076-0.
[19] S.B. Oblath, S.S. Markowitz, T. Novakov, S.G. Chang, Reaction of nitrite Ion with Hydroxylamine-N-sulfonate in aqueous solution, Inorg. Chem. 22 (1983) 579–583, https://doi.org/10.1021/ic00146a002.
[20] T. Tacke, Dissertation, Tech. Univ. Carolo-Wilhelmina. (1991). https://doi.org/10.1016/0039-6028(91)90317-L.
[21] J. Wärn, I. Turunen, T. Salmi, T. Maunula, Kinetics of nitrate reduction in monolith reactor, Chem. Eng. Sci. 49 (1994) 5763–5773, https://doi.org/10.1016/0009-2509(94)00331-9.
[22] E.E.A. (EEA), https://www.eea.europa.eu/data-and-maps/figures/nitrate-concentration-in-groundwater, (2002). https://doi.org/10.1016/0039-6028(91)

90317-L.
[23] M. Vospernik, A. Pintar, G. Berčič, J. Levec, Experimental verification of ceramic membrane potentials for supporting three-phase catalytic reactions, J. Memb. Sci. 223 (2003) 157–169, https://doi.org/10.1016/S0376-7388(03)00320-X.
[24] K.T. Ranjit, B. Viswanathan, Photocatalytic reduction of nitrite and nitrate ions to ammonia on M/TiO2 catalysts, J. Photochem. Photobiol. A: Chem. 108 (1997) 73–78, https://doi.org/10.1016/S1010-6030(96)04505-4.
[25] C. Franch, R.G.H. Lammertink, L. Lefferts, Partially hydrophobized catalyst particles for aqueous nitrite hydrogenation, Appl. Catal. B Environ. 156–157 (2014) 166–172, https://doi.org/10.1016/j.apcatb.2014.03.020.
[26] Y. Zhao, L. Jia, J.A. Medrano, J.R.H. Ross, L. Lefferts, Supported Pd catalysts prepared via colloidal method: the effect of acids, ACS Catal. 3 (2013) 2341–2352, https://doi.org/10.1021/cs4004479.
[27] A.M. Bergquist, M. Bertoch, G. Gildert, T.J. Strathmann, C.J. Werth, Catalytic denitrification in a trickle bed reactor: ion exchange waste brine treatment, J. Am. Water Works Assoc. 109 (2017) E129–E143, https://doi.org/10.5942/jawwa.2017.109.0055.
[28] H.C. Aran, S. Pacheco Benito, M.W.J. Luiten-Olieman, S. Er, M. Wessling, L. Lefferts, N.E. Benes, R.G.H. Lammertink, Carbon nanofibers in catalytic membrane microreactors, J. Memb. Sci. 381 (2011) 244–250, https://doi.org/10.1016/j.memsci.2011.07.037.
[29] V. Hessel, P. Angeli, A. Gavriilidis, H. Löwe, Gas − liquid and gas − liquid − solid microstructured reactors: contacting principles and applications, Ind. Eng. Chem. Res. 44 (2005) 9750–9769, https://doi.org/10.1021/ie0503139.
[30] M.J. Geerken, T.S. van Zanten, R.G.H. Lammertink, Z. Borneman, W. Nijdam, C.J.M. van Rijn, M. Wessling, Chemical and thermal stability of alkylsilane based coatings for membrane emulsification, Adv. Eng. Mater. 6 (2004) 749–754, https://doi.org/10.1002/adem.200400060.
[31] A. Quintanilla, J.J.W.W. Bakker, M.T. Kreutzer, J.A. Moulijn, F. Kapteijn, Tuning the support adsorption properties of Pd/SiO2 by silylation to improve the selective hydrogenation of aromatic ketones, J. Catal. 257 (2008) 55–63, https://doi.org/10.1016/j.jcat.2008.04.006.
[32] C. Grote, M. Rosu, A. Schumpe, The effect of Pd-catalyst wettability on hydrogenation of nitrate to hydroxylamine, Can. J. Chem. Eng. 88 (2010) 633–637, https://doi.org/10.1002/cjce.20312.
[33] H. Yang, X. Jiao, S. Li, Hydrophobic core-hydrophilic shell-structured catalysts: a general strategy for improving the reaction rate in water, Chem. Commun. (Camb.) 48 (2012) 11217–11219, https://doi.org/10.1039/c2cc36273b.
[34] A. Perro, F. Meunier, V. Schmitt, S. Ravaine, Production of large quantities of "Janus" nanoparticles using wax-in-water emulsions, Colloids Surf. A Physicochem. Eng. Asp. 332 (2009) 57–62, https://doi.org/10.1016/j.colsurfa.2008.08.027.
[35] J. Faria, M.P. Ruiz, D.E. Resasco, Phase-selective catalysis in emulsions stabilized by Janus silica-nanoparticles, Adv. Synth. Catal. 352 (2010) 2359–2364, https://doi.org/10.1002/adsc.201000479.
[36] R. Brunet Espinosa, D. Rafieian, R.S. Postma, R.G.H. Lammertink, L. Lefferts, Eggshell membrane reactors for nitrite hydrogenation: manipulating kinetics and selectivity, Appl. Catal. B Environ. 224 (2018) 276–282, https://doi.org/10.1016/j.apcatb.2017.10.058.
[37] S.D. Ebbesen, B.L. Mojet, L. Lefferts, In situ ATR-IR study of nitrite hydrogenation over Pd/Al2O3, J. Catal. 256 (2008) 15–23, https://doi.org/10.1016/j.jcat.2008.02.013.
[38] R. Zhang, D. Shuai, K.A. Guy, J.R. Shapley, T.J. Strathmann, C.J. Werth, Elucidation of nitrate reduction mechanisms on a Pd-In bimetallic catalyst using isotope labeled nitrogen species, ChemCatChem 5 (2013) 313–321, https://doi.org/10.1002/cctc.201200457.
[39] I. Mikami, Y. Sakamoto, Y. Yoshinaga, T. Okuhara, Kinetic and adsorption studies on the hydrogenation of nitrate and nitrite in water using Pd-Cu on active carbon support, Appl. Catal. B Environ. 44 (2003) 79–86, https://doi.org/10.1016/S0926-3373(03)00021-3.
[40] U. Hanefeld, L. Lefferts, Catalysis: an integrated textbook, Focus Catal. 2017 (2017) 7, https://doi.org/10.1016/j.focat.2017.11.046.
[41] Pengyu Xu, Shilpa Agarwal, Leon Lefferts, Mechanism of nitrite hydrogenation over Pd/γ-Al2O3 according a rigorous kinetic study, (n.d.).
[42] D.M. Shuai, J.K. Choe, J.R. Shapley, C.J. Werth, J. Charles, C.J. Werth, Enhanced activity and selectivity of carbon nanofiber supported Pd catalysts for nitrite reduction, Environ. Sci. Technol. 46 (2012) 2847–2855, https://doi.org/10.1021/es203200d.
[43] F. Deganello, L.F. Liotta, A. Macaluso, A.M. Venezia, G. Deganello, Catalytic reduction of nitrates and nitrites in water solution on pumice-supported Pd-Cu catalysts, Appl. Catal. B Environ. 24 (2000) 265–273, https://doi.org/10.1016/S0926-3373(99)00109-5.
[44] R.S. Postma, R. Brunet Espinosa, L. Lefferts, Competitive adsorption of nitrite and hydrogen on palladium during nitrite hydrogenation, ChemCatChem 10 (2018) 3770–3776, https://doi.org/10.1002/cctc.201800523.
[45] Y. Zhao, N. Koteswara Rao, L. Lefferts, Adsorbed species on Pd catalyst during nitrite hydrogenation approaching complete conversion, J. Catal. 337 (2016) 102–110, https://doi.org/10.1016/j.jcat.2016.02.007.
[46] W. Sun, W. Yang, Z. Xu, Q. Li, J.K. Shang, Synthesis of superparamagnetic core-shell structure supported Pd nanocatalysts for catalytic nitrite reduction with enhanced activity, No detection of undesirable product of ammonium, and easy magnetic separation capability, ACS Appl. Mater. Interfaces 8 (2016) 2035–2047, https://doi.org/10.1021/acsami.5b10365.